Journal of Power Sources 205 (2012) 385–393

Contents lists available at SciVerse ScienceDirect

Journal of Power Sources

journal homepage: www.elsevier.com/locate/jpowsour

Electrochemical investigations of the $LiNi_{0.45}M_{0.10}Mn_{1.45}O_4$ (M = Fe, Co, Cr) 5 V cathode materials for lithium ion batteries

G.B. Zhong, Y.Y. Wang, Y.Q. Yu, C.H. Chen*

CAS Key Laboratory of Materials for Energy Conversion, Department of Materials Science and Engineering, University of Science and Technology of China, Anhui, Hefei 230026, China

ARTICLE INFO

Article history:
Received 30 September 2011
Received in revised form
15 December 2011
Accepted 19 December 2011
Available online 16 January 2012

Keywords:
Lithium ion batteries
Spinel
Trivalent transition metal doping
Lithium nickel manganese oxide
Thermopolymerization

ABSTRACT

$LiNi_{0.5}Mn_{1.5}O_4$ and $LiNi_{0.45}M_{0.10}Mn_{1.45}O_4$ (M = Fe, Co, Cr) powders are prepared and systematically investigated as 5 V cathode materials for lithium-ion batteries. X-ray diffraction, Raman spectroscopy and scanning electron microscopy are employed to study their structures. The electrochemical cyclic performance and rate capability at room temperature and 55 °C are characterized and compared. The results indicate that the introductions of Fe, Co or Cr ions favor the crystal structure of the spinel in a $Fd\bar{3}m$ symmetry compared with a symmetry of $P4_332$ for the un-doped $LiNi_{0.5}Mn_{1.5}O_4$. Excellent cycle life is measured for these 5 V Co- and Fe-doped electrodes. When cycled at 1C rate, about 95.9%, 93.1% and 81.7% of their initial capacities can be retained after 500 cycles for $LiNi_{0.45}Co_{0.10}Mn_{1.45}O_4$, $LiNi_{0.45}Fe_{0.10}Mn_{1.45}O_4$ and $LiNi_{0.45}Cr_{0.10}Mn_{1.45}O_4$, respectively. Their electrochemical performances at 55 °C are also much better than the un-doped sample. Three possible capacity fading mechanisms including structural transformation, the dissolution of the spinel into the electrolyte, and the oxidation of the electrolyte are discussed. The decomposition of the electrolyte is regarded as the most important mechanism.

1. Introduction

$LiNi_{0.5}Mn_{1.5}O_4$ has been extensively studied as a cathode material for lithium ion batteries during the past decade [1–21]. In recent years it has attracted even more attentions because of its high operating potential (4.7 V vs. lithium) and three dimensional lithium-ion diffusion paths in the spinel lattice. Lithium ion batteries with $LiNi_{0.5}Mn_{1.5}O_4$-based positive electrodes are expected to provide high power/energy density for electric vehicles (EVs), hybrid electric vehicles (HEVs) and large energy storage systems. $LiNi_{0.5}Mn_{1.5}O_4$ has two different crystal structures of $P4_332$ and $Fd\bar{3}m$, depending on the oxygen content in the lattice and/or the degree of ordering of the Ni/Mn ions [5,6]. A high-temperature (>700 °C) synthesis usually leads to produce a $LiNi_{0.5}Mn_{1.5}O_4$ powder with the $Fd\bar{3}m$ structure. In this structure, Ni and Mn ions are randomly distributed in the 16d sites, while some of the oxygen is released out of its lattice structure and a small amount of Mn^{4+} ions are reduced to Mn^{3+} to balance the charge. An annealing of the spinel powder at 700 °C in air can transform its crystal structure from $Fd\bar{3}m$ to $P4_332$, in which the Ni and Mn ions occupy orderly on the 4a and 12d sites, respectively. During the charging/discharging processes, $LiNi_{0.5}Mn_{1.5}O_4$ demonstrates two plateaus at around 4.7 V, corresponding to the redox reactions of Ni^{2+}/Ni^{3+} and Ni^{3+}/Ni^{4+} couples. Kim et al. [6] studied the phase transition of $LiNi_{0.5}Mn_{1.5}O_4$ during Li^+ extraction by measuring the ex situ XRD patterns. They have found that the $LiNi_{0.5}Mn_{1.5}O_4$ with a space group of $Fd\bar{3}m$ undergoes a topotactic two-phase transition during electrochemical cycling, while the $LiNi_{0.5}Mn_{1.5}O_4$ with a space group of $P4_332$ shows topotactic phase transitions among three different cubic phases. Recently, Wang et al. [21] studied the phase evolution during Li insertion/extraction process using in situ XRD. They have observed three cubic phases for the $LiNi_{0.5}Mn_{1.5}O_4$ samples with either $P4_332$ or $Fd\bar{3}m$ structure. For the $LiNi_{0.5}Mn_{1.5}O_4$ with a $Fd\bar{3}m$ structure, an additional 4.0 V plateau may be observed that is corresponding to the Mn^{3+}/Mn^{4+} redox couple. According to Ariyoshi et al. [5], the $LiNi_{0.5}Mn_{1.5}O_4$ with the $Fd\bar{3}m$ structure exhibits better electrochemical performances than that with the $P4_332$ structure.

On the other hand, it is difficult to synthesize a pure stoichiometric $LiNi_{0.5}Mn_{1.5}O_4$ because an impurity phase $Li_yNi_{1-y}O$ tends to be formed during the high temperature synthesis [22,23]. Besides, the fast capacity fading of a $LiNi_{0.5}Mn_{1.5}O_4$ electrode at elevated temperatures is another disadvantage of this material for applications [24,25].

To improve the electrochemical performance, various modification methods such as lattice doping and surface coating [15,24,26–28] have been adopted. Partial substitutions of Mn and (or) Ni in $LiMn_{1.5}Ni_{0.5}O_4$ with other cations such as Al [29], Mg [30,31], Ti [32], Cr [9,17,33], Fe [34], Co [35,36], Cu [37], Zn [38], and Ru [16] have been investigated. It has been found that the cationic

* Corresponding author. Tel.: +86 551 3606971.
E-mail address: cchchen@ustc.edu.cn (C.H. Chen).

0378-7753/$ – see front matter © 2011 Elsevier B.V. All rights reserved.
doi:10.1016/j.jpowsour.2011.12.037

substitutions can eliminate the formation of the $Li_yNi_{1-y}O$ impurity phase and stabilize the spinel structure with a disordering of the Mn^{4+} and Ni^{2+} ions in the 16d octahedral sites. Such a cationic doping also results in a smaller difference in lattice parameter among the three cubic phases formed during the cycling process so that the cycle life is prolonged.

Among the various cationic substitutions, Liu and co-worker [34] have investigated the substitution of Fe for Ni alone or both for Ni and Mn. They have found that $LiMn_{1.5}Ni_{0.42}Fe_{0.08}O_4$ exhibits a capacity retention of 100% after 100 cycles and a remarkably high capacity of 106 mAh g^{-1} at 10C rate. Ito et al. [35] have synthesized $LiNi_{0.5-x}Co_{2x}Mn_{1.5-x}O_4$ ($0 \le 2x \le 0.2$) by spray drying and found that the Co substitution for Ni and Mn result in improved electrochemical performances at a high rate and at elevated temperatures. Liu et al. [17] have investigated the influence of Cr content on the electrochemical performance of $LiNi_{0.5-x}Cr_{2x}Mn_{1.5-x}O_4$ and optimized the Cr concentration in the range $0.05 \le 2x \le 0.10$. Although all the Fe-, Co- and Cr-doping can improve the performance of the $LiNi_{0.5}Mn_{1.5}O_4$, it is difficult to determine which is the most effective from these literatures because the synthesis methods and test standards are different from group to group. In this study, we have synthesized a series of trivalent transition-metal doped $LiNi_{0.45}M_{0.10}Mn_{1.45}O_4$ (M = Fe, Co, Cr) powders by the same thermopolymerization method. Their electrochemical performances are tested and compared to develop an in-depth understanding of the impacts of the cationic doping with trivalent transition metals.

2. Experimental

The $LiNi_{0.5}Mn_{1.5}O_4$ and $LiNi_{0.45}M_{0.10}Mn_{1.45}O_4$ (M = Fe, Co, Cr) powders were synthesized by a thermopolymerization method [10]. Stoichiometric amounts of lithium nitrate ($LiNO_3$, 5% excess), ferric nitrate ($Fe(NO_3)_3{\cdot}9H_2O$), cobalt nitrate ($Co(NO_3)_2{\cdot}6H_2O$), chromium nitrate ($Cr(NO_3)_3{\cdot}9H_2O$), nickel nitrate ($Ni(NO_3)_2{\cdot}6H_2O$) and manganese acetate ($Mn(CH_3COO)_2{\cdot}4H_2O$) were dissolved in deionized water to obtain a 0.2 M solution. Then acrylic acid (AA) was added to form an AA–H_2O (1:2, v/v) solution. The solution was kept in an oven at 150 °C for 10 h to proceed thermopolymerization reactions. The intermediate gel-like products were first calcined at 500 °C for 10 h, and then cooled down to room temperature. After being grinded, the obtained powders were sintered at 900 °C for 15 h and subsequently annealed at 700 °C for 48 h. All the heat treatment processes were carried out in air atmosphere.

The powders obtained after the high temperature sintering and 700 °C annealing were analyzed by X-ray diffraction (XRD) using a diffractometer (Philips X'pert Pro Super, Cu Kα radiation) at room temperature. The XRD patterns were recorded in the 2θ range from 10° to 80°, with step 0.05° and speed 2° min^{-1}. The Raman spectra of the $LiNi_{0.5}Mn_{1.5}O_4$ and $LiNi_{0.45}M_{0.10}Mn_{1.45}O_4$ (M = Fe, Co, Cr) samples were also collected with a Confocal Laser Micro Raman Spectrometer (LABRAM-HR, Jobin Yvon) using an excitation light of 514.5 nm from Ar ion laser (the excitation power is less than 1.0 mW). To have more reliable data, each Raman spectrum was the average of 3 scans collected at a spectral resolution of 2.0 cm^{-1}. The particle size and morphology were also observed under a scanning electron microscope (JSM-6390LA, JEOL).

To prepare the electrode laminates, the spinel active materials, acetylene black and poly(vinylidene fluoride) (PVDF) (80:10:10, w/w/w) were mixed into slurries in N-methyl-2-pyrrolidone in an agate mortar. They were then cast on aluminum foils with a doctor blade and dried at 70 °C for 10 h to obtain several electrode laminates. Discs (ϕ = 14 mm) of the laminates were punched, dried at 70 °C for 2 h in a vacuum oven and then were transferred into an argon-filled glove box (MBraun Labmaster 130). A typical electrode mass was 4.5–5.5 mg. Afterwards, CR2032 type coin-cells with Li as the counter electrode were assembled in the glove box with the electrolyte of 1 M $LiPF_6$ solution in ethylene carbonate (EC)–dimethyl carbonate (DMC) (1:1, w/w, Zhuhai Smoothway Electronics Materials Co., Ltd.).

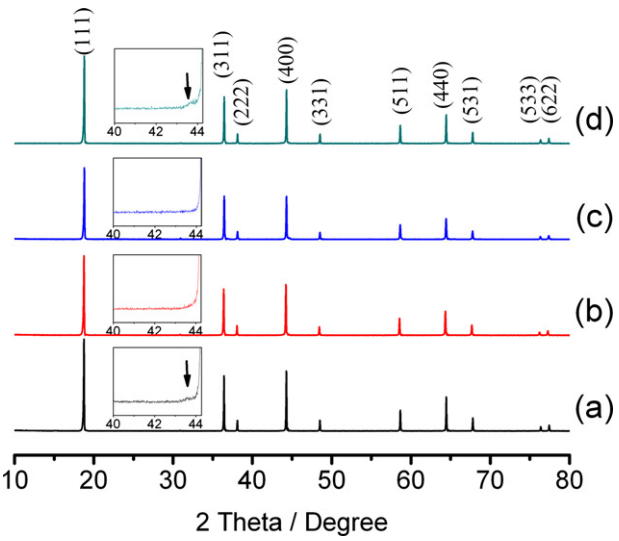

Fig. 1. X-ray diffraction patterns of (a) $LiNi_{0.5}Mn_{1.5}O_4$; (b) $LiNi_{0.45}Fe_{0.10}Mn_{1.45}O_4$; (c) $LiNi_{0.45}Co_{0.10}Mn_{1.45}O_4$; (d) $LiNi_{0.45}Cr_{0.10}Mn_{1.45}O_4$. The $LiNi_{0.5}Mn_{1.5}O_4$ is of $P4_332$ structure while the doped samples are of $Fd\bar{3}m$ structure. A weak peak attributed to rock salt impurity (NiO or $Li_yNi_{1-y}O$) is observed in the magnified patterns of $LiNi_{0.5}Mn_{1.5}O_4$ and $LiNi_{0.45}Cr_{0.10}Mn_{1.45}O_4$.

The cyclic voltammograms (CV) of the batteries were measured on a CHI 604A electrochemical workstation from 3.5 to 5.1 V at a scan rate of 0.1 mV s^{-1}. The batteries were also galvanostatically cycled on a multi-channel battery cycler (Neware BTS2300, Shenzhen) in the voltage window from 3.5 to 5.0 V. The room temperature is controlled at 25 °C (±3 °C) by an air-conditioner. The high temperature performances of the cells were tested by laying them in an oven at 55 °C (±1 °C).

The possible dissolution of the transition-metal ions into the electrolyte was tested by soaking the electrodes in 2.0 ml electrolyte and storing them in a 55 °C oven for a week. Then, the concentrations of the transition-metal ions in the electrolyte were measured using an inductively coupled plasma atomic emission spectrometer (ICP) (Optima 7300 DV, Perkin-Elmer Co., USA).

3. Results and discussion

3.1. Crystal structures and particle morphology of the $LiNi_{0.5}Mn_{1.5}O_4$ and the $LiNi_{0.45}M_{0.10}Mn_{1.45}O_4$ (M = Fe, Co, Cr) powders

Fig. 1 presents the X-ray diffraction patterns of the synthesized powders. The $LiNi_{0.5}Mn_{1.5}O_4$ powder has been indexed by the cubic $P4_332$ symmetry due to the appearances of the weak peaks located at 2θ = 15.3°, 39.7°, 45.7°, and 57.5°, while these peaks are absent from the pattern of $Fd\bar{3}m$ structure. However, the Fe-, Co- and Cr-doped samples are indexed by $Fd\bar{3}m$ space group. In addition, the inset figures in Fig. 1 show the magnified patterns between 40° and 44.25°. A weak peak attributed to the impurity NiO or $Li_yNi_{1-y}O$ is observed in the patterns of $LiNi_{0.5}Mn_{1.5}O_4$ and $LiNi_{0.45}Cr_{0.10}Mn_{1.45}O_4$, but absent in the other two patterns. This implies that the doping of Fe and Co may effectively suppress the formation of impurities. Considering that the additional XRD peaks for space group $P4_332$ are too weak, Raman spectroscopy is adopted to distinguish the $P4_332$ from the $Fd\bar{3}m$ space group. As is shown in Fig. 2, the Raman spectrum of the undoped $LiNi_{0.5}Mn_{1.5}O_4$

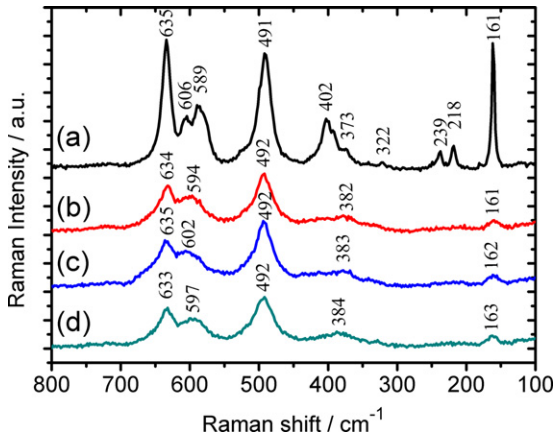

Fig. 2. Raman spectra for (a) $LiNi_{0.5}Mn_{1.5}O_4$; (b) $LiNi_{0.45}Fe_{0.10}Mn_{1.45}O_4$; (c) $LiNi_{0.45}Co_{0.10}Mn_{1.45}O_4$; (d) $LiNi_{0.45}Cr_{0.10}Mn_{1.45}O_4$. The spectra of the doped spinels ($Fd\bar{3}m$) are different from that of the pristine $LiNi_{0.5}Mn_{1.5}O_4$ ($P4_332$).

is different from those of the doped samples $LiNi_{0.45}M_{0.10}Mn_{1.45}O_4$ (M = Fe, Co, Cr). According to Oh et al. [29] and Julien and co-worker [39], the strong band around 635 cm^{-1} is assigned to the symmetric Mn–O stretching mode of MnO_6 octahedra (A_{1g}). Both peaks around 402 and 491 cm^{-1} are associated with the Ni^{2+}–O stretching mode in the structure. And the peak near 580–606 cm^{-1} is considered as $T_{2g}^{(3)}$ of the spinel compound. In addition, the peak splitting between the bands at 606 and 589 cm^{-1} is clearly observed for $LiNi_{0.5}Mn_{1.5}O_4$, while only a broad hump is observed for the doped samples. Also, the bands around 400, 239, 218 and 160 cm^{-1} are much stronger for the $LiNi_{0.5}Mn_{1.5}O_4$ than for the doped samples. Note that the splitting of $T_{2g}^{(3)}$ band is often considered as the obvious evidence of the ordered structure ($P4_332$) of the spinel. Meanwhile, the strong bands around 400, 239, 218 and 161 cm^{-1} are also the features of $P4_332$ structure. Therefore, it can be concluded that the introductions of Fe, Co or Cr ions favor the formation of $Fd\bar{3}m$ structure.

Fig. 3 shows the scanning electron microscopy (SEM) images of the $LiNi_{0.5}Mn_{1.5}O_4$ and $LiNi_{0.45}M_{0.10}Mn_{1.45}O_4$ (M = Fe, Co, Cr) powders. It can be found that the particle morphologies of these spinel powders are almost the same. The particles exhibit clean and smooth surface facets, which suggest that the samples are all well crystallized. The average particle size of these powders is around 2.0 μm.

3.2. Cyclic behaviors of the $LiNi_{0.5}Mn_{1.5}O_4$ and the $LiNi_{0.45}M_{0.10}Mn_{1.45}O_4$ (M = Fe, Co, Cr) at room temperature

Fig. 4 shows the cyclic voltammograms of the cells with the $LiNi_{0.5}Mn_{1.5}O_4$ and $LiNi_{0.45}M_{0.10}Mn_{1.45}O_4$ (M = Fe, Co, Cr) spinels as the working electrodes. It can be observed in Fig. 4a that the $LiNi_{0.5}Mn_{1.5}O_4$ shows only a strong peak at 4.84 V and 4.60 V, corresponding to the oxidation and reduction reactions of Ni^{2+}/Ni^{4+}. However, in the case of the doped samples in Fig. 4b–d, the strong peak splits into two peaks, locating at 4.75 V/4.82 V in the oxidation process and 4.68 V/4.60 V in the reduction process. This is because the voltage difference between Ni^{2+}/Ni^{3+} and Ni^{3+}/Ni^{4+} redox couples in $Fd\bar{3}m$ spinel is greater than that in $P4_332$ spinel. For $LiNi_{0.45}Fe_{0.10}Mn_{1.45}O_4$ (Fig. 4b) and $LiNi_{0.45}Cr_{0.10}Mn_{1.45}O_4$ (Fig. 4d), there is an additional high-voltage redox peak at around 4.9 V, which should be attributed to the Fe^{3+}/Fe^{4+} and Cr^{3+}/Cr^{4+} redox reactions, respectively. Similar results have been reported by Ohzuku et al. [1] and Sigala et al. [40]. Moreover, because the peak at 4.0 V is due to the Mn^{3+}/Mn^{4+} redox reaction, the amounts of Mn^{3+} in the spinels can be roughly estimated by comparing the integrated area of the peak around 4.0 V with the area of the peaks around 4.8 V. The calculated amount of Mn^{3+} is 0.034 in a unit formula $LiNi_{0.5}Mn_{1.5}O_4$. As a contrast, the amounts of Mn^{3+} are as

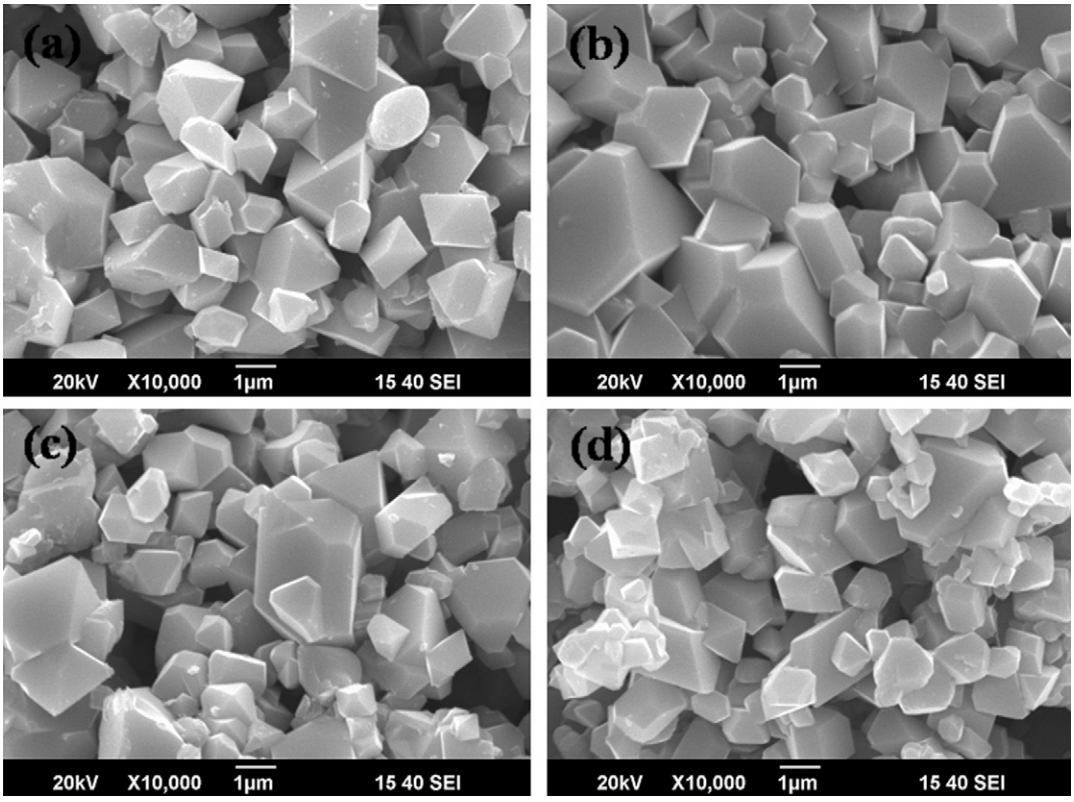

Fig. 3. SEM images of (a) $LiNi_{0.5}Mn_{1.5}O_4$; (b) $LiNi_{0.45}Fe_{0.10}Mn_{1.45}O_4$; (c) $LiNi_{0.45}Co_{0.10}Mn_{1.45}O_4$; (d) $LiNi_{0.45}Cr_{0.10}Mn_{1.45}O_4$.

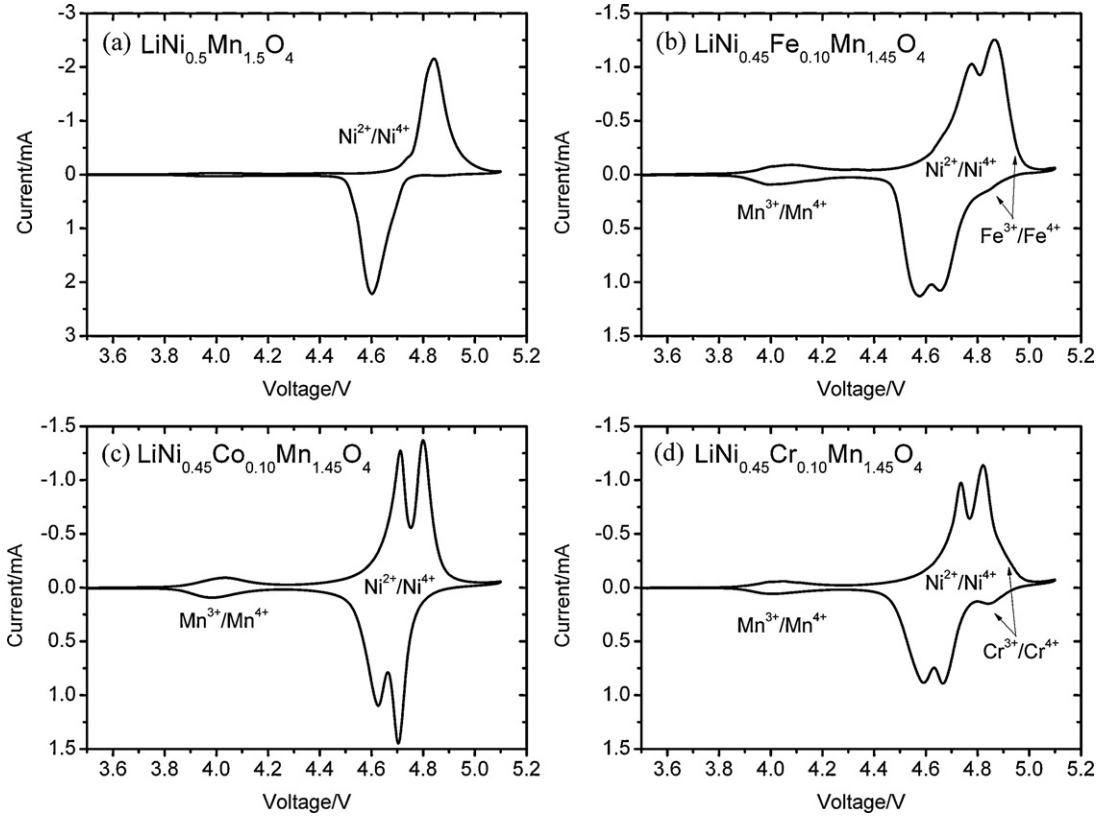

Fig. 4. Cyclic voltammograms of (a) $LiNi_{0.5}Mn_{1.5}O_4$; (b) $LiNi_{0.45}Fe_{0.10}Mn_{1.45}O_4$; (c) $LiNi_{0.45}Co_{0.10}Mn_{1.45}O_4$; (d) $LiNi_{0.45}Cr_{0.10}Mn_{1.45}O_4$.

high as 0.096, 0.092 and 0.072 in Fe-, Co- and Cr-doped spinels, respectively.

The cycling stabilities of the samples at room temperature are tested by galvanostatically charging/discharging the cells under a current density of 140 mA g^{-1} (0.45 mA cm^{-2} or 1C rate) for 500 cycles. As shown in Fig. 5, the undoped $LiNi_{0.5}Mn_{1.5}O_4$ delivers an initial discharge capacity of about 133 mAh g^{-1} and a capacity of 63 mAh g^{-1} at the 500th cycle, with the capacity retention of 47% after 500 cycles. On the other hand, although the doped samples $LiNi_{0.45}M_{0.10}Mn_{1.45}O_4$ (M = Fe, Co, Cr) have similar theoretical capacity compared with $LiNi_{0.5}Mn_{1.5}O_4$, they deliver different reversible capacities as the substituent M is either electrochemically active or inert in the measured voltage window (3.5–5.0 V).

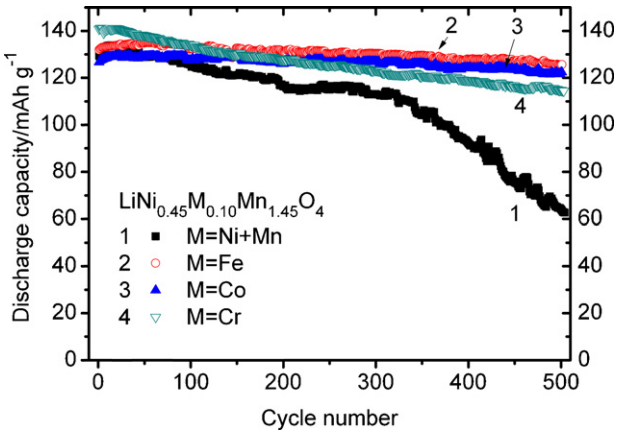

Fig. 5. Cyclic performance of (a) $LiNi_{0.5}Mn_{1.5}O_4$; (b) $LiNi_{0.45}Fe_{0.10}Mn_{1.45}O_4$; (c) $LiNi_{0.45}Co_{0.10}Mn_{1.45}O_4$ and (d) $LiNi_{0.45}Cr_{0.10}Mn_{1.45}O_4$ at room temperature. The cycling tests were carried out under the current density of 140 mA g^{-1} (0.45 mA cm^{-2} or 1C rate).

According to Ohzuku et al. [1] and Kawai et al. [41,42], the redox potential of Co^{3+}/Co^{4+} reaction in $LiCo_xMn_{2-x}O_4$ is around 5.1 V (vs. Li^+/Li). Thus, the Co^{3+} in the Co-doped sample is electrochemically inactive in the voltage range from 3.5 to 5.0 V. The $LiNi_{0.45}Co_{0.10}Mn_{1.45}O_4$ electrode in this study delivers an initial capacity of about 130 mAh g^{-1}, which is slightly lower than that of $LiNi_{0.5}Mn_{1.5}O_4$. However, for the $LiNi_{0.45}Fe_{0.10}Mn_{1.45}O_4$ and $LiNi_{0.45}Cr_{0.10}Mn_{1.45}O_4$ with the contributions of Fe^{3+}/Fe^{4+} and Cr^{3+}/Cr^{4+} reactions at the voltage > 4.9 V, they deliver initial capacities of 135 mAh g^{-1} and 140 mAh g^{-1}, respectively, which are higher than the pristine $LiNi_{0.5}Mn_{1.5}O_4$. Moreover, the cycling stability of the $LiNi_{0.5}Mn_{1.5}O_4$ is significantly improved by the Fe-, Co- and Cr-doping. The capacity retention increases to 81.7% after 500 cycles for the $LiNi_{0.45}Cr_{0.10}Mn_{1.45}O_4$ electrode. Very remarkably, the $LiNi_{0.45}Fe_{0.10}Mn_{1.45}O_4$ and the $LiNi_{0.45}Co_{0.10}Mn_{1.45}O_4$ have even superior cycling performance, retaining 93.1% and 95.9% of their initial capacities, respectively, after 500 cycles.

To have an exhaustive understanding on the changes during the prolonged cycling process, the voltage profiles of the $LiNi_{0.5}Mn_{1.5}O_4$ and $LiNi_{0.45}M_{0.10}Mn_{1.45}O_4$ (M = Fe, Co, Cr) spinels at the 1st, 100th, 300th, and 500th cycles are presented in Fig. 6. The charge/discharge profiles are significantly different for the pristine $LiNi_{0.5}Mn_{1.5}O_4$ and the doped samples. The $LiNi_{0.5}Mn_{1.5}O_4$ exhibits a charge/discharge plateau with an average potential of 4.70 V, corresponding to the redox reaction of Ni^{2+}/Ni^{4+} in the $P4_332$ structure (Fig. 6a). However, two plateaus at 4.76 V and 4.65 V are clearly observed for the doped spinel samples (Fig. 6b–d). The two flat plateaus are corresponding to the two-phase coexistences of ($LiNi_{0.45}M_{0.10}Mn_{1.45}O_4 + Li_{0.45}Ni_{0.45}M_{0.10}Mn_{1.45}O_4$) and ($Li_{0.45}Ni_{0.45}M_{0.10}Mn_{1.45}O_4 + Li_{0.10}Ni_{0.45}M_{0.10}Mn_{1.45}O_4$), respectively. Therefore, during the charge/discharge processes, totally three spinel phases appear, i.e. $LiNi_{0.45}M_{0.10}Mn_{1.45}O_4$,

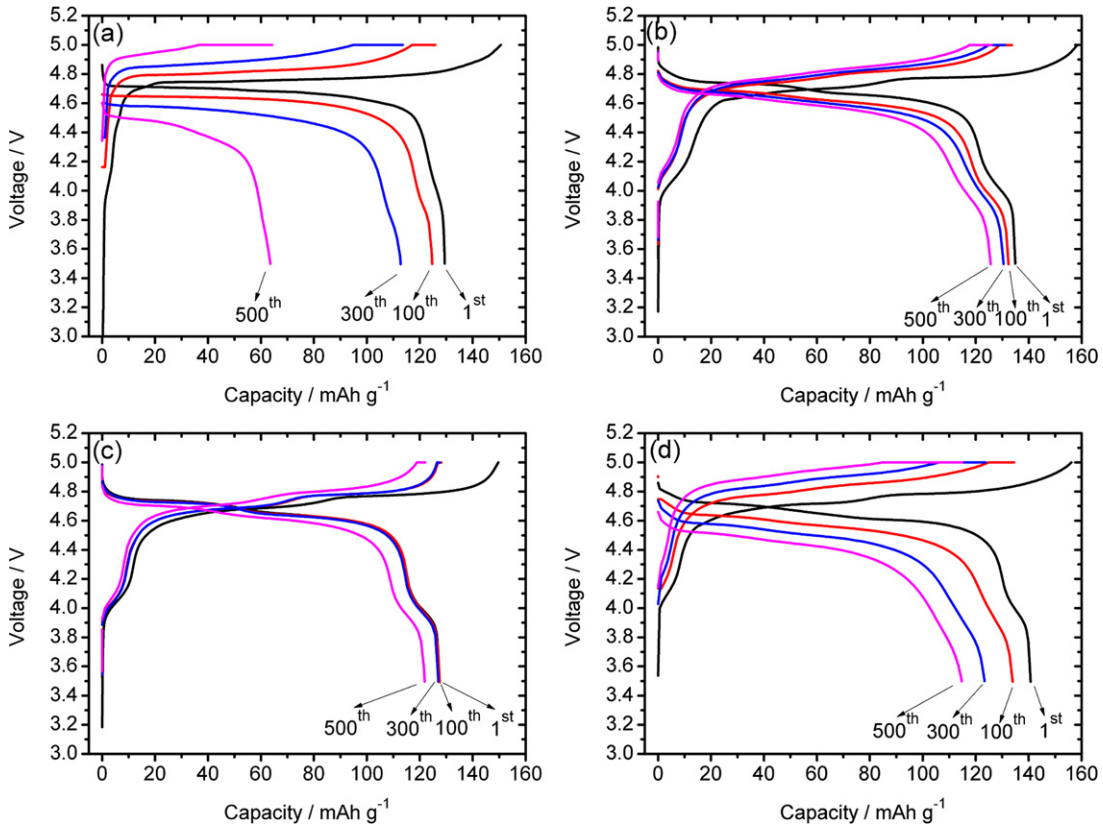

Fig. 6. Voltage profiles of (a) $LiNi_{0.5}Mn_{1.5}O_4$; (b) $LiNi_{0.45}Fe_{0.10}Mn_{1.45}O_4$; (c) $LiNi_{0.45}Co_{0.10}Mn_{1.45}O_4$ and (d) $LiNi_{0.45}Cr_{0.10}Mn_{1.45}O_4$ at the 1st, 100th, 300th, and 500th cycles at room temperature. The pristine $LiNi_{0.5}Mn_{1.5}O_4$ and the $LiNi_{0.45}Cr_{0.10}Mn_{1.45}O_4$ electrodes suffer from significant increase in the polarization and severe capacity fading.

$Li_{0.45}Ni_{0.45}M_{0.10}Mn_{1.45}O_4$ and $Li_{0.10}Ni_{0.45}M_{0.10}Mn_{1.45}O_4$. This is consistent with the in situ analysis results by Wang et al. [21].

With increasing the cycle number, the pristine $LiNi_{0.5}Mn_{1.5}O_4$ (Fig. 6a) and $LiNi_{0.45}Cr_{0.10}Mn_{1.45}O_4$ (Fig. 6d) suffer from significant polarization increase and severe capacity fading. The increased polarization may be caused by the possible electrolyte decomposition at high potentials. The decomposition products can coat on the surface of the electrodes and hinder the lithium transport, lead to increased polarization. As a contrast, the polarization is substantially suppressed in the Fe- and Co-doped samples, because excellent stability is achieved in the cells of $LiNi_{0.45}M_{0.10}Mn_{1.45}O_4$/Li (M = Fe, Co) during the prolonged cycling.

3.3. Cyclic behaviors of the $LiNi_{0.5}Mn_{1.5}O_4$ and the $LiNi_{0.45}M_{0.10}Mn_{1.45}O_4$ (M = Fe, Co, Cr) at 55 °C

$LiNi_{0.5}Mn_{1.5}O_4$ spinel may experience severe capacity loss when cycling at an elevated temperature (50–60 °C) [24,25]. Here, the results of 55 °C-cycling at 1C rate on these samples are shown in Fig. 7. It can be seen that the pristine $LiNi_{0.5}Mn_{1.5}O_4$ indeed suffers from a rapid capacity fading from 132.4 mAh g^{-1} to 100.6 mAh g^{-1}, or with only 76.0% retention, after 200 cycles. On the contrary, the $LiNi_{0.45}Fe_{0.10}Mn_{1.45}O_4$ and $LiNi_{0.45}Co_{0.10}Mn_{1.45}O_4$ electrodes display a greatly improved cyclic performance with a capacity of

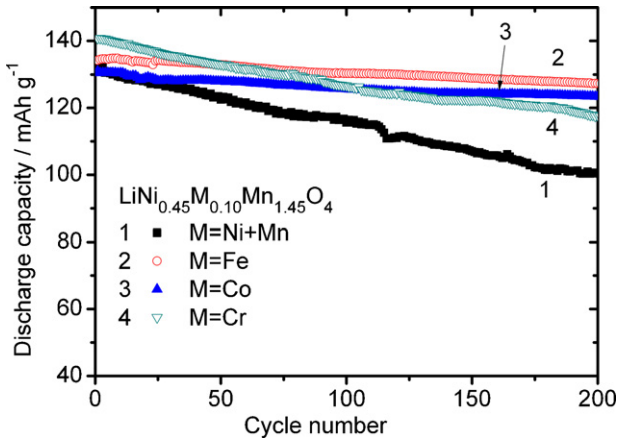

Fig. 7. Cyclic performance of (1) $LiNi_{0.5}Mn_{1.5}O_4$; (2) $LiNi_{0.45}Fe_{0.10}Mn_{1.45}O_4$; (3) $LiNi_{0.45}Co_{0.10}Mn_{1.45}O_4$ and (4) $LiNi_{0.45}Cr_{0.10}Mn_{1.45}O_4$ at 55 °C. The cycling tests were carried out under the current density of 140 mA g^{-1} (0.45 mA cm^{-2} or 1C rate).

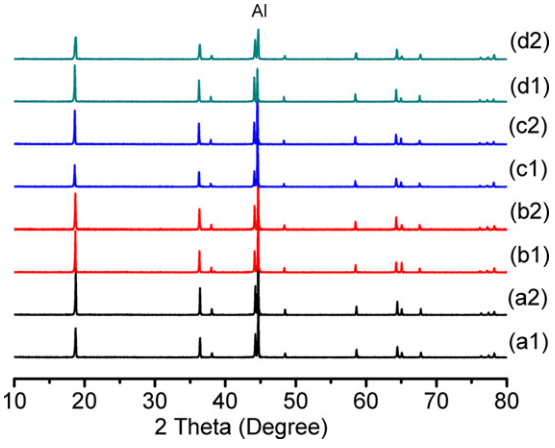

Fig. 8. X-ray diffraction patterns of the electrodes of (a2) $LiNi_{0.5}Mn_{1.5}O_4$; (b2) $LiNi_{0.45}Fe_{0.10}Mn_{1.45}O_4$; (c2) $LiNi_{0.45}Co_{0.10}Mn_{1.45}O_4$; (d2) $LiNi_{0.45}Cr_{0.10}Mn_{1.45}O_4$ after 200 cycles at 55 °C. The patterns of the fresh electrodes (a1, b1, c1, d1) are also presented for comparison.

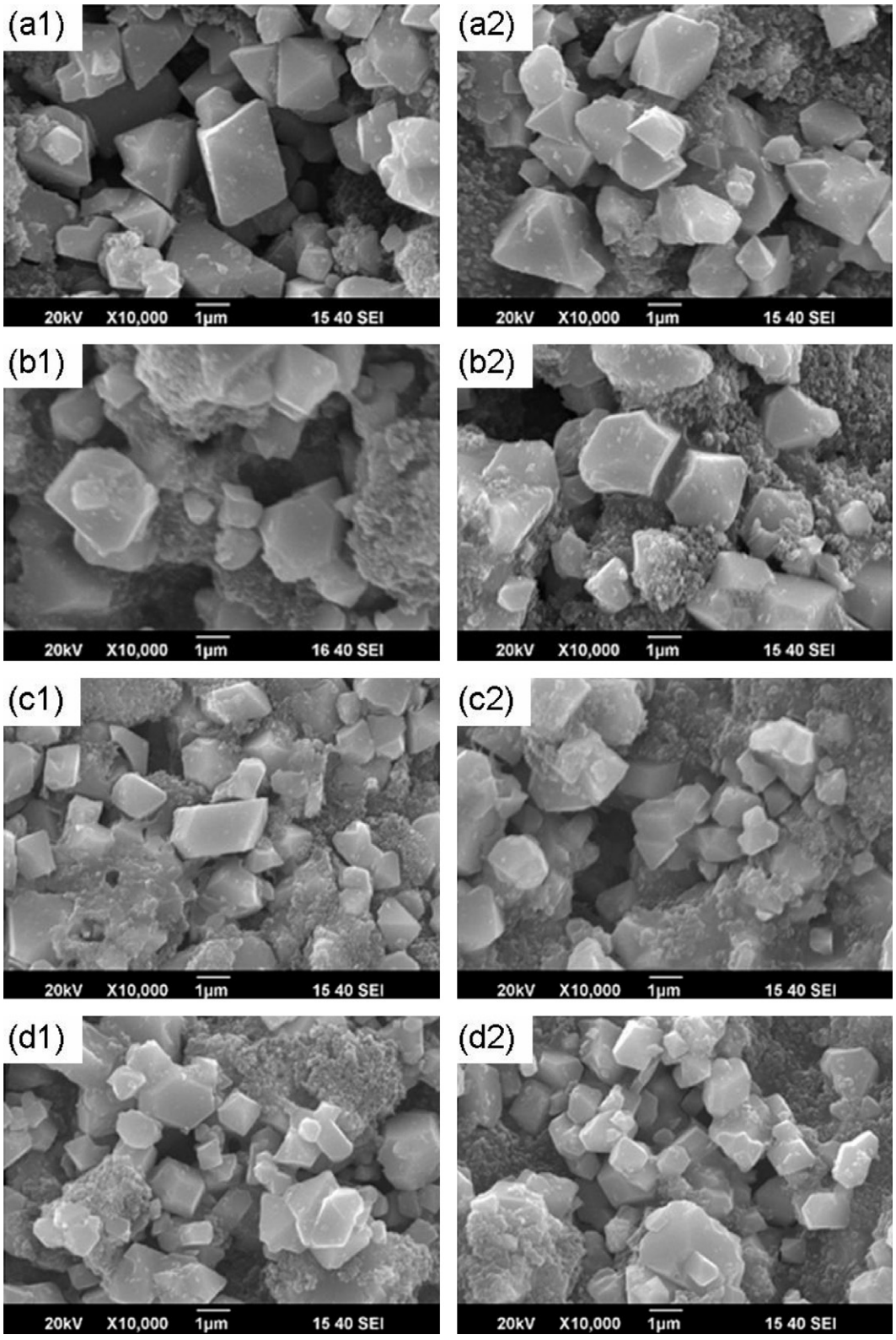

Fig. 9. SEM images of the electrodes before and after 200 cycles at 55 °C: $LiNi_{0.5}Mn_{1.5}O_4$ (a1, a2), $LiNi_{0.45}Fe_{0.10}Mn_{1.45}O_4$ (b1, b2), $LiNi_{0.45}Co_{0.10}Mn_{1.45}O_4$ (c1, c2) and $LiNi_{0.45}Cr_{0.10}Mn_{1.45}O_4$ (d1, d2). No obvious changes in the morphology are observed before and after electrochemical cycling.

127.3 and 123.4 mAh g^{-1} (94.9% and 94.3% of their initial capacity), respectively, after 200 cycles. The $LiNi_{0.45}Cr_{0.10}Mn_{1.45}O_4$ maintains 83.6% of its initial capacity after 200 cycles at 55 °C, which is inferior compared with the Fe- and Co-doped samples, but superior to the pristine $LiNi_{0.5}Mn_{1.5}O_4$.

3.4. Capacity fading mechanisms of the $LiNi_{0.5}Mn_{1.5}O_4$ and the $LiNi_{0.45}M_{0.10}Mn_{1.45}O_4$ (M = Fe, Co, Cr)

Generally, the key factors that cause the capacity fading of $LiNi_{0.5}Mn_{1.5}O_4$-based cathodes are: (i) structural transformation

during cycling, (ii) the dissolution of the spinel into the electrolyte, and (iii) the oxidation of the electrolyte during charging. To observe any structural changes during the cycling, the cells were disassembled after 200 cycles at 55 °C and the positive electrodes were analyzed by XRD and SEM. The fresh electrodes (a1, b1, c1 and d1) were also examined to be compared with their corresponding cycled electrodes (a2, b2, c2 and d2). As is shown in their XRD patterns (Fig. 8), all the samples present well-defined cubic spinels patterns without any obvious changes compared with the fresh electrodes. The strong peak at 44.6° is due to Al current collector. The morphology of the $LiNi_{0.5}Mn_{1.5}O_4$ and $LiNi_{0.45}M_{0.10}Mn_{1.45}O_4$ (M = Fe, Co, Cr) electrodes before and after 200 cycles at 55 °C is shown in Fig. 9. The surface facet morphologies are maintained for all the samples. These results suggest that no obvious structural transformation takes place during the electrochemical cycling so it should not be the main cause of capacity fading.

To investigate the possible dissolution of the spinel into the electrolyte, the positive electrodes before cycling were soaked in 2.0 ml electrolyte in sealed vials and then placed in a 55 °C oven for a week. Then the contents of Mn, Fe, Co and Cr in the electrolyte solution were measured by means of ICP analysis. The results are listed in Table 1. It seems that the contents of Mn dissolved in the solution have a corresponding relationship with the amounts of Mn^{3+} in the spinels (as specified in Fig. 4). When more Mn^{3+} ions exist in the spinel, more soluble Mn^{2+} ions can be produced by the disproportionation reaction $2Mn^{3+} \rightarrow Mn^{2+} + Mn^{4+}$. On the other hand, the dissolution of the doping elements (Fe, Co and Cr) is so little (<2.0 μg ml^{-1}) that it should not be the main reason for the capacity fading. Otherwise, the $LiNi_{0.5}Mn_{1.5}O_4$ would have showed the best cycling stability, because the cation dissolution for this sample is the lowest (Table 1).

The last suspect is the oxidation of the electrolyte. The photos of the electrodes after 200 cycles at 55 °C confirm this speculation. As is shown in Fig. 10, some gray deposits are found on the surfaces of the Li electrodes for both the $LiNi_{0.5}Mn_{1.5}O_4$/Li and $LiNi_{0.45}Fe_{0.10}Mn_{1.45}O_4$/Li cells. After the cell disassembly, the positive electrode laminate and the separator membrane were found to be nearly dry in the $LiNi_{0.5}Mn_{1.5}O_4$/Li cell while they were still moist in the $LiNi_{0.45}Fe_{0.10}Mn_{1.45}O_4$/Li cell. This means that the oxidation of the electrolyte in the $LiNi_{0.5}Mn_{1.5}O_4$/Li cell is more severe than that in the $LiNi_{0.45}Fe_{0.10}Mn_{1.45}O_4$/Li cell. As also shown in Fig. 6, the pristine $LiNi_{0.5}Mn_{1.5}O_4$ electrode and the $LiNi_{0.45}Cr_{0.10}Mn_{1.45}O_4$ electrode suffer from severe polarization so that more electrolyte may be oxidized due to the higher voltages in the charging process.

3.5. Rate performances of the $LiNi_{0.5}Mn_{1.5}O_4$ and the $LiNi_{0.45}M_{0.10}Mn_{1.45}O_4$ (M = Fe, Co, Cr)

To compare the rate capabilities of the $LiNi_{0.5}Mn_{1.5}O_4$ and the $LiNi_{0.45}M_{0.10}Mn_{1.45}O_4$ (M = Fe, Co, Cr) spinels, all of the cells were galvanostatically charged at room temperature under a current density of 70 mA g^{-1} (0.5C rate) and discharged under different current densities from 70 mA g^{-1} (0.5C rate) to 1400 mA g^{-1} (10C rate) and then back to 70 mA g^{-1}. Fig. 11 shows the voltage profiles of the $LiNi_{0.5}Mn_{1.5}O_4$ and $LiNi_{0.45}M_{0.10}Mn_{1.45}O_4$ (M = Fe, Co, Cr) electrodes at different C rates. The pristine $LiNi_{0.5}Mn_{1.5}O_4$ shows a capacity loss from 133 mAh g^{-1} at 0.2C to 45 mAh g^{-1} at 10C, with the average discharge voltage decreasing from 4.69 V to 3.67 V (Fig. 11a). As a contrast, all of the doped samples show significantly improved rate performances. The $LiNi_{0.45}Fe_{0.10}Mn_{1.45}O_4$ and $LiNi_{0.45}Cr_{0.10}Mn_{1.45}O_4$ can deliver remarkably high capacity of 121 mAh g^{-1} and 130 mAh g^{-1}, respectively, at 10C rate, which are 90% and 92% of their capacities at 0.2C rate. Their average discharge voltage at 10C is still kept at about 4.3 V (Fig. 11b and d). The $LiNi_{0.45}Co_{0.10}Mn_{1.45}O_4$ electrode performs even better, because a discharge capacity of 124 mAh g^{-1} (97.6% of its capacity at 0.2C) is maintained at 10C rate, with a high average discharge voltage of 4.50 V (Fig. 11c). The discharge capacity values at various C-rates are plotted in Fig. 12a. Clearly, the rate capability increases in the order of $LiNi_{0.5}Mn_{1.5}O_4 < LiNi_{0.45}Fe_{0.10}Mn_{1.45}O_4 \approx LiNi_{0.45}Cr_{0.10}Mn_{1.45}O_4 < LiNi_{0.45}Co_{0.10}Mn_{1.45}O_4$. Moreover, the results of capacity and discharge voltage can be presented in the form of energy density contributed from the positive electrodes (i.e. only the mass of the positive electrode materials being counted) (Fig. 12b). The results show the same trend with Fig. 12a, indicating that the trivalent transition-metal doping is an effective method to improve the rate performance of $LiNi_{0.5}Mn_{1.5}O_4$.

The improvement in the rate performance should be related to the conductivity increase caused by the trivalent

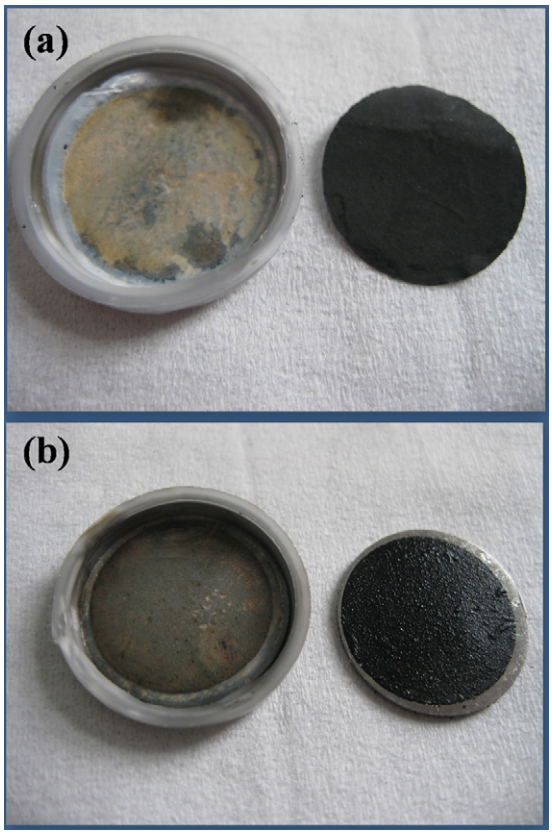

Fig. 10. Photos of the Li and positive electrodes of (a) $LiNi_{0.5}Mn_{1.5}O_4$/Li and (b) $LiNi_{0.45}Fe_{0.10}Mn_{1.45}O_4$/Li batteries after 200 cycles at 55 °C.

Table 1
ICP results of the dissolution of transition metal ions in the electrolyte solution.

Samples	Mn (μg ml^{-1})	Fe (μg ml^{-1})	Co (μg ml^{-1})	Cr (μg ml^{-1})
$LiNi_{0.5}Mn_{1.5}O_4$	9.40	–	–	–
$LiNi_{0.45}Fe_{0.10}Mn_{1.45}O_4$	15.04	1.82	–	–
$LiNi_{0.45}Co_{0.10}Mn_{1.45}O_4$	14.16	–	0.35	
$LiNi_{0.45}Cr_{0.10}Mn_{1.45}O_4$	12.24	–		1.20

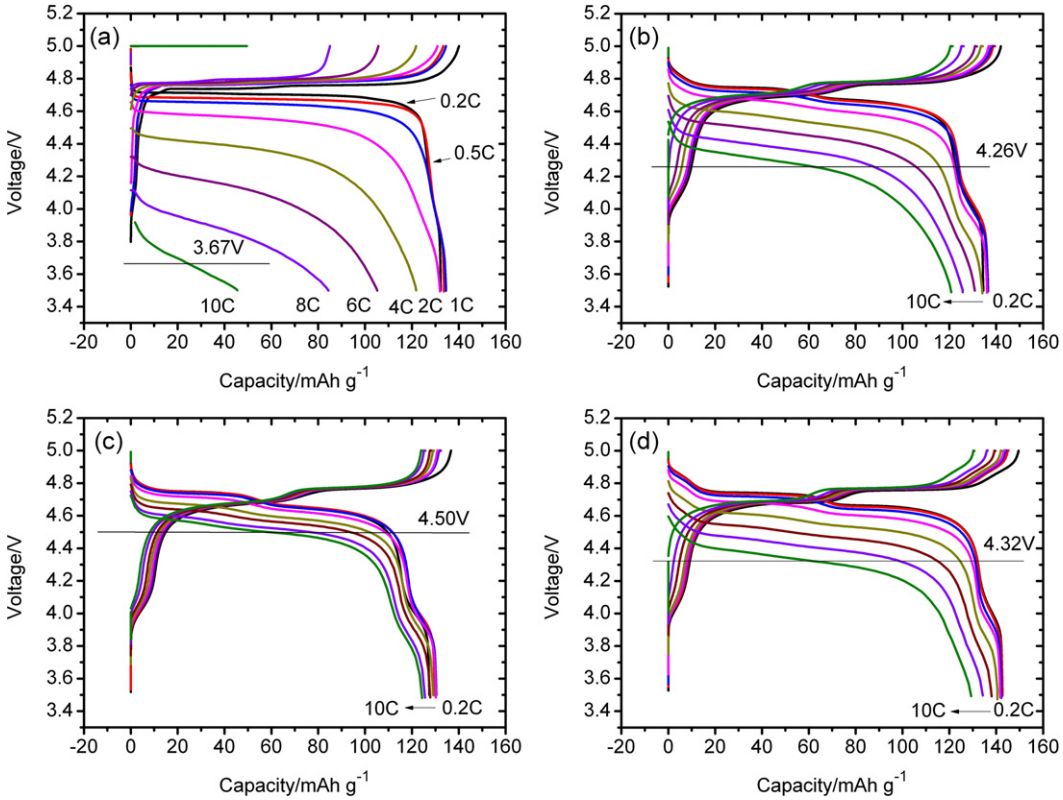

Fig. 11. Voltage profiles of (a) $LiNi_{0.5}Mn_{1.5}O_4$; (b) $LiNi_{0.45}Fe_{0.10}Mn_{1.45}O_4$; (c) $LiNi_{0.45}Co_{0.10}Mn_{1.45}O_4$ and (d) $LiNi_{0.45}Cr_{0.10}Mn_{1.45}O_4$ at different C rates at room temperature. The cells were charged under a current density of 70 mA g^{-1} (0.5C rate) and discharged under different current densities from 70 mA g^{-1} (0.5C rate) to 1400 mA g^{-1} (10C rate).

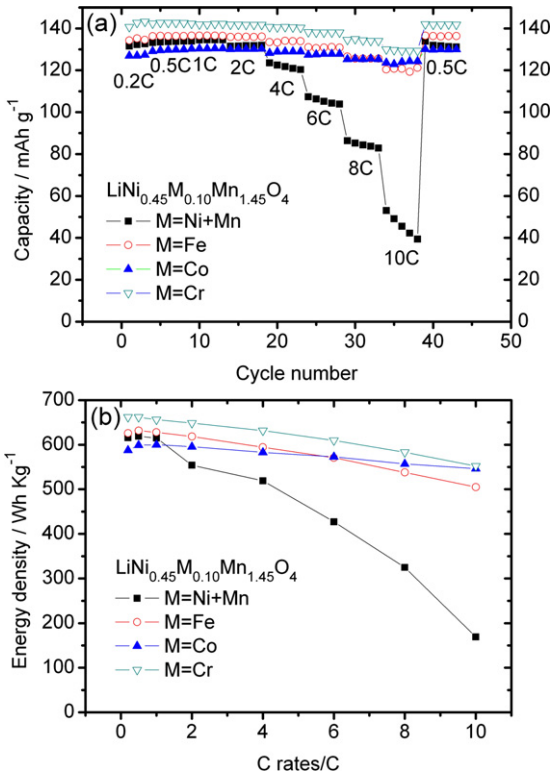

Fig. 12. (a) Discharge capacity values and (b) energy density values of the pristine $LiNi_{0.5}Mn_{1.5}O_4$ and $LiNi_{0.45}M_{0.10}Mn_{1.45}O_4$ (M = Fe, Co, Cr) spinels at various C rates from 0.5C to 10C. The doped spinels exhibit significantly improved rate performance compared with the undoped $LiNi_{0.5}Mn_{1.5}O_4$.

transition-metal doping. To prove this speculation, the DC resistances of the batteries were measured during the 4th discharge process, by employing a current interruption for 1.0 min after every discharge step for 5.0 min. The values of the calculated resistance of the batteries vs. the depth of discharge (DOD) are given in Fig. 13. The "W"-shape curves are observed, indicating the conversions of $Ni^{4+} \rightarrow Ni^{3+}$ and $Ni^{3+} \rightarrow Ni^{2+}$ of the spinels during the discharge process. This phenomenon is consistent with our previous report [10]. Obviously, all of the trivalent transition-metal doped spinels demonstrate lower resistances than the pristine $LiNi_{0.5}Mn_{1.5}O_4$. The great difference of the DC resistance must be originated from the difference in their structures. Kunduraci et al. [43] have found that the $P4_332$ phase of $LiNi_{0.5}Mn_{1.5}O_4$ presents a lower electronic conductivity, with a value of 10^{-7} S cm^{-1} at room temperature, compared with 10^{-5} S cm^{-1} for the $Fd\bar{3}m$ phase. In Fig. 13, the

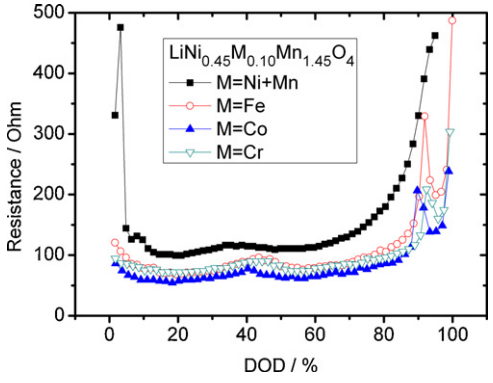

Fig. 13. DC resistances as a function of DOD for the $LiNi_{0.5}Mn_{1.5}O_4$ and $LiNi_{0.45}M_{0.10}Mn_{1.45}O_4$ (M = Fe, Co, Cr) spinels. The much higher DC resistance of $LiNi_{0.5}Mn_{1.5}O_4$ is due to its $P4_332$ structure and it is the cause of poor rate performance.

DC resistance decreases in the order of $LiNi_{0.5}Mn_{1.5}O_4 > LiNi_{0.45}Fe_{0.10}Mn_{1.45}O_4 \approx LiNi_{0.45}Cr_{0.10}Mn_{1.45}O_4 > LiNi_{0.45}Co_{0.10}Mn_{1.45}O_4$, which is exactly the reverse order of their rate capability (Fig. 12).

4. Conclusions

The $LiNi_{0.5}Mn_{1.5}O_4$ and the $LiNi_{0.45}M_{0.10}Mn_{1.45}O_4$ (M = Fe, Co, Cr) spinel powders have been synthesized by a thermopolymerization method. The introductions of these trivalent transition-metal elements in the lattice favor the change of the space group of $LiNi_{0.5}Mn_{1.5}O_4$ from ordered $P4_332$ to disordered $Fd\bar{3}m$. The Fe- and Cr-doping can increase the specific capacity of the $LiNi_{0.5}Mn_{1.5}O_4$ while the Co-doping causes slight reduction in the initial capacity. All of the trivalent transition-metal dopings can significantly improve the cycling stability of the $LiNi_{0.5}Mn_{1.5}O_4$ electrode. At room temperature, the 1C-capacity retentions after 500 cycles increase from 47% for the undoped sample to 93.1%, 95.9% and 81.7% for the Fe-, Co- and Cr-doped samples, respectively. At 55 °C, the capacity retentions after 200 cycles increase from 76.0% for the undoped sample to 94.9%, 94.3% and 83.6% for the Fe-, Co- and Cr-doped samples, respectively. Moreover, the rate capability of the $LiNi_{0.5}Mn_{1.5}O_4$ is also greatly improved by the trivalent transition-metal doping. When discharged at 10C rate, the $LiNi_{0.45}Fe_{0.10}Mn_{1.45}O_4$ and the $LiNi_{0.45}Cr_{0.10}Mn_{1.45}O_4$ maintain over 90% of their capacity at 0.2C rate. The $LiNi_{0.45}Co_{0.10}Mn_{1.45}O_4$ performs even better because a discharge capacity of 124 mAh g^{-1} (capacity retention of 97.6%) is maintained at 10C rate with a high average discharge voltage of 4.50 V. The oxidation of the electrolyte solution may be the main cause of the capacity fading at elevated temperatures. The DC resistance tests confirm that the trivalent transition-metal doping can increase the electronic conductivity, leading to an improvement in the rate capability.

Acknowledgements

This study was supported by National Science Foundation of China (grant no. 20971117, 10979049 and J1030412) and Education Department of Anhui Province (grant no. KJ2009A142). We are also grateful to the Solar Energy Operation Plan of Academia Sinica.

References

[1] T. Ohzuku, S. Takeda, M. Iwanaga, J. Power Sources 82 (1999) 90.
[2] Y.S. Lee, Y.K. Sun, S. Ota, T. Miyashita, M. Yoshi, Electrochem. Commun. 4 (2002) 989.
[3] M. Mohamedi, A. Makino, K. Dokko, T. Itoh, I. Uchida, Electrochim. Acta 48 (2002) 79.
[4] Y. Idemoto, H. Narai, N. Koura, J. Power Sources 119 (2003) 125.
[5] K. Ariyoshi, Y. Iwakoshi, N. Nakayama, T. Ohzuku, J. Electrochem. Soc. 151 (2004) A296.
[6] J.H. Kim, S.T. Myung, C.S. Yoon, S.G. Kang, Y.K. Sun, Chem. Mater. 16 (2004) 906.
[7] B. Markovsky, Y. Talyossef, G. Salitra, D. Aurbach, H.J. Kim, S. Choi, Electrochem. Commun. 6 (2004) 821.
[8] D. Kovacheva, B. Markovsky, G. Salitra, Y. Talyosef, M. Gorova, E. Levi, M. Riboch, H.J. Kim, D. Aurbach, Electrochim. Acta 50 (2005) 5553.
[9] T.A. Arunkumar, A. Manthiram, Electrochim. Acta 50 (2005) 5568.
[10] H.Y. Xu, S. Xie, N. Ding, B.L. Liu, Y. Shang, C.H. Chen, Electrochim. Acta 51 (2006) 4352.
[11] M. Kunduraci, G.G. Amatucci, J. Power Sources 165 (2007) 359.
[12] J.C. Arrebola, A. Caballero, L. Hernan, J. Morales, J. Power Sources 180 (2008) 852.
[13] H.F. Xiang, X. Zhang, Q.Y. Jin, C.P. Zhang, C.H. Chen, X.W. Ge, J. Power Sources 183 (2008) 355.
[14] M. Aklalouch, R.M. Rojas, J.M. Rojo, I. Saadoune, J.M. Amarilla, Electrochim. Acta 54 (2009) 7542.
[15] J. Liu, A. Manthiram, Chem. Mater. 21 (2009) 1695.
[16] H.L. Wang, H. Xia, M.O. Lai, L. Lu, Electrochem. Commun. 11 (2009) 1539.
[17] D.Q. Liu, Y.H. Lu, J.B. Goodenough, J. Electrochem. Soc. 157 (2010) A1269.
[18] B. Rambabu, R. Santhanam, J. Power Sources 195 (2010) 5442.
[19] N. Amdouni, K. Zaghib, F. Gendron, A. Mauger, C.M. Julien, Ionics 12 (2006) 117.
[20] N. Amdouni, K. Zaghib, F. Gendron, A. Mauger, C.M. Julien, J. Magn. Magn. Mater. 309 (2007) 100.
[21] L.P. Wang, H. Li, X.J. Huang, E. Baudrin, Solid State Ionics 193 (2011) 32.
[22] Q.M. Zhong, A. Bonakdarpour, M.J. Zhang, Y. Gao, J.R. Dahn, J. Electrochem. Soc. 144 (1997) 205.
[23] R. Alcantara, M. Jaraba, P. Lavela, J.L. Tirado, Electrochim. Acta 47 (2002) 1829.
[24] Y.K. Sun, Y.S. Lee, M. Yoshio, K. Amine, Electrochem. Solid State Lett. 5 (2002) A99.
[25] H.M. Wu, J.P. Tu, Y.F. Yuan, Y. Li, X.B. Zhao, G.S. Cao, Electrochim. Acta 50 (2005) 4104.
[26] Y.K. Sun, K.J. Hong, J. Prakash, K. Amine, Electrochem. Commun. 4 (2002) 344.
[27] Y.K. Sun, C.S. Yoon, I.H. Oh, Electrochim. Acta 48 (2003) 503.
[28] J.S. Kim, C.S. Johnson, J.T. Vaughey, S.A. Hackney, K.A. Walz, W.A. Zeltner, M.A. Anderson, M.M. Thackeray, J. Electrochem. Soc. 151 (2004) A1755.
[29] S.H. Oh, K.Y. Chung, S.H. Jeon, C.S. Kim, W.I. Cho, B.W. Cho, J. Alloys Compd. 469 (2009) 244.
[30] M. Wagemaker, F.G.B. Ooms, E.M. Kelder, J. Schoonman, G.J. Kearley, F.M. Mulder, J. Am. Chem. Soc. 126 (2004) 13526.
[31] C. Locati, U. Lafont, L. Simonin, F. Ooms, E.M. Kelder, J. Power Sources 174 (2007) 847.
[32] R. Alcantara, M. Jaraba, P. Lavela, J.L. Tirado, P. Biensan, A. de Guibert, C. Jordy, J.P. Peres, Chem. Mater. 15 (2003) 2376.
[33] M. Aklalouch, J.M. Amarilla, R.M. Rojas, I. Saadoune, J.M. Rojo, J. Power Sources 185 (2008) 501.
[34] J. Liu, A. Manthiram, J. Phys. Chem. C 113 (2009) 15073.
[35] A. Ito, D. Li, Y. Lee, K. Kobayakawa, Y. Sato, J. Power Sources 185 (2008) 1429.
[36] S.W. Oh, S.T. Myung, H.B. Kang, Y.K. Sun, J. Power Sources 189 (2009) 752.
[37] G.T.K. Fey, C.Z. Lu, T.P. Kumar, J. Power Sources 115 (2003) 332.
[38] J. Liu, A. Manthiram, J. Electrochem. Soc. 156 (2009) A66.
[39] C.M. Julien, M. Massot, Mater. Sci. Eng. B: Solid 97 (2003) 217.
[40] C. Sigala, A. Verbaere, J.L. Mansot, D. Guyomard, Y. Piffard, M. Tournoux, J. Solid State Chem. 132 (1997) 372.
[41] H. Kawai, M. Nagata, H. Tukamoto, A.R. West, Electrochem. Solid State Lett. 1 (1998) 212.
[42] A.R. West, H. Kawai, M. Nagata, H. Kageyama, H. Tukamoto, Electrochim. Acta 45 (1999) 315.
[43] M. Kunduraci, J.F. Al-Sharab, G.G. Amatucci, Chem. Mater. 18 (2006) 3585.